Double grazing bifurcation route in a quasiperiodically driven piecewise linear oscillator

Run Liu[a], Grebogi Celso[b], Yuan Yue [c,*]

[a, c] Applied Mechanics and Structure Safety Key Laboratory of Sichuan Province, School of Mechanics and Aerospace Engineering, Southwest Jiaotong University, Chengdu 610031, China

[b] Institute for Complex Systems and Mathematical Biology King's College, University of Aberdeen, Aberdeen; AB24 3UE, United Kingdom

Abstract

Considering a piecewise linear oscillator with quasiperiodic excitation, we uncover the route of the double grazing bifurcation of quasiperiodic torus to strange nonchaotic attractors (i.e., SNAs). The maximum displacement for double grazing bifurcation of the quasiperiodic torus can be obtained analytically. After the double grazing of the quasiperiodic orbits, the smooth quasiperiodic torus wrinkles increasingly with the continuous change of the parameter. Subsequently, the whole quasiperiodic torus loses the somoothness by becoming everywhere non-differentiable, which indicates the birth of SNAs. The Lyapunov exponent is adopted to verify the nonchaotic property of the SNA. The strange property of SNAs is characterized by the phase sensitivity, the power spectrum, the singular continuous spectrum, and the fractal structure. Our detailed analysis shows that the SNAs induced by the double grazing may exist in a short parameter interval between 1T quasiperiodic orbit and 2T quasiperiodic orbit, or between 1T quasiperiodic orbit and 4T quasiperiodic orbit, or between 1T quasiperiodic orbit and chaotic motion. Noteworthy, SNAs may also exist in a large parameter interval after double grazing, which does not lead to any quasiperiodic or chaotic orbits.

Keyword: Piecewise linear oscillator; Strange nonchaotic attractors; Quasiperiodic torus; Double grazing bifurcation; Fractal.

* Corresponding author.

E-mail addresses: leyuan2003@sina.com (Yuan Yue), run139315@163.com (Run Liu), grebogi@adbn.ac.uk (Grebogi, Celso).

1. Introduction

Grazing bifurcation leads to various kinds of nonclassical bifurcations in the vibro-impact systems, such as typical period-adding bifurcation, period-adding bifurcation with bands of chaos and creation of an intermittent chaos. Whiston [1-2] firstly adopted singularity theory to study the non-differentiability of the Poincaré mapping near the grazing point, and analyzed the reason for the singularity generated by the breaking of stable manifolds. Shaw et al. [3] considered a class of elastically constrained impact vibration systems, and found that the zero-velocity impact is the cause of the singularity of the Poincaré map. Based on Whiston's work, Chillingworth [4-5] proposed a discontinuous geometric analysis method for a generic one degree of freedom impact oscillator, and systematically discussed degenerate (cubic) grazing. Jiang et al. [6] used the discontinuous geometric method and a numerical simulation method to discuss in detail the existence conditions of periodic solutions of an impact oscillator with one-sided elastic constraint. Kryzhevich et al. [7] studied a second-order differential equation with periodic coefficients from the topological perspective and proved that chaotic invariant set occurs when the system parameters are changed continuously at the grazing bifurcation point. By means of numerical stability analysis and experimental verification, Banerjee et al. [8] discovered a narrow band of chaos close to the grazing condition for a simple soft impact oscillator. In Ref. [9], GPU parallel computing technology was used to study the two-parameter dynamics problem in the vicinity of grazing bifurcation points.

Nordmark [10] considered rigidly constrained impact oscillator with periodic excitation, and introduced the concept of discontinuity map to study the singularity of the system caused by grazing bifurcations by virtue of analytical methods. In Ref. [11], Nordmark analyzed the universal limit mapping of a kind of impact oscillator when the eigenvalues are real numbers, and converted the system into the form of interval mapping. He proved that there is no periodic orbit when the maximum eigenvalue is greater than two-thirds, and the limit mapping for any parameter is in chaotic state. Chin et al. [12] studied a simple sinusoidally forced oscillator system in the presence of friction and a hard wall, and identified three kinds of codimension one bifurcations when the eigenvalues are complex. Considering a class of micro-driven devices, Dankowicz et al. [13] proposed three types of co-dimension one bifurcation, and predicted the dynamic characteristics by

using discontinuous mapping method. By means of the sequence limit theory, Zhang [14] derived the discontinuous maps of a rub-impacting rotor system to analyze the bifurcation situation induced by grazing. Feng [15] adopted the graph cell mapping theory to study the global dynamics of the grazing-induced crisis of the Duffing system. Brzeski [16] studied the grazing bifurcation problem of a kind of church pendulum model with clearance, and revealed a new grazing bifurcation phenomenon different from the period adding motion, namely, "impact adding" phenomenon.

In 1984, Grebogi et al. [17] uncovered a new attractor which owns both strange and nonchaotic properties, and named it "strange nonchaotic attractor" (i.e., SNA), and gave the dynamical definition of SNA. SNAs has been extensively investigated theoretically, numerically and experimentally. Both SNAs and chaotic attractors have the strange property [18]. Although SNAs are geometrically strange (i.e., fractal), they exhibit no sensitive dependence on initial conditions, and have non-positive maximum Lyapunov exponents (i.e., nonchaotic) [19]. Moreover, SNAs have sensitive dependence on initial phase, which can be characterized by the phase sensitivity, indicating the strange property [20]. In recent years, the generation mechanism of SNAs has attracted the attention of many scholars. Mitsui et al. [21] discussed the existence of SNAs generated by the intermittent path in a particular non-skew-product map related to quasiperiodically driven continuous dynamical systems. By means of nonlinear dynamical analysis and numerical evidence, Zhang et al. [22] found SNAs in the periodically driven noisy FHN neuron model. Li et al. [23] considered a periodically forced nonsmooth system and found that noise-induced SNAs can be generated by periodic attractors near the boundary crisis. Shen et al. [24] studied the mechanisms for the creation of strange nonchaotic attractors in a quasiperiodic forced piecewise logistic system, and uncovered the Heagy-Hammel routes, fractalization route and intermittent routes after the two coexisting tori collide. Zhang et al. [25] initially identified an unusual route for the creation of a SNA in a quasiperiodic forced interval map at the grazing bifurcation point, and then compared the difference between the grazing bifurcation route and the fractalization route path.

The present study aims at uncovering the routes of the double grazing bifurcation of quasiperiodic torus to SNAs in a quasiperiodic forced piecewise linear oscillator. The remaining of this paper is organized as follows. In Sec. 2, the model of the piecewise linear oscillator is introduced and the maximum displacement of the double grazing bifurcation of the quasiperiodic torus is

obtained. Then the piecewise linear system is transformed into a three-dimensional Poincaré map by selecting a suitable Poincaré section. In Sec. 3, dynamical measures are represented to characterize SNAs, including maximal Lyapunov exponent, phase sensitivity, power spectrum, and singular continuous spectrum. In Sec. 4, various SNAs induced by double grazing bifurcation of quasiperiodic orbits are obtained by numerical simulations. In Sec. 5, the strange property of the SNAs is characterized by its phase sensitivity, power spectrum, singular continuous spectrum, as well as fractal structure. Finally, we give the conclusions in Sec. 6.

2. The piecewise linear oscillator with quasiperiodic excitation

The physical model of the piecewise linear oscillator is shown in Fig. 1. The mass *m* is attached to a linear damper with damping coefficient *c*, and two linear springs with stiffness coefficients K_1 and K_2, respectively. Figure 2 describes the restoring force of the spring K_2 by means of a piecewise linear function. The interval between the mass and the spring K_2 is *G*, which is symmetric. The quasiperiodic excitation $A\cos(\Omega_1 t) + B\cos(\Omega_2 t)$ is applied to the mass, where the ratio of Ω_1 over Ω_2 is an irrational number.

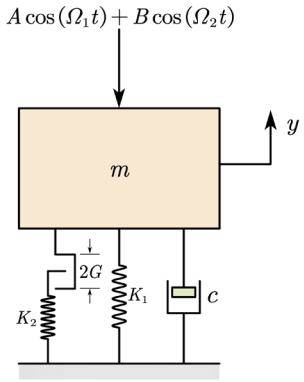

Fig. 1. Piecewise linear oscillator.

The differential equation of motion is

$$m\ddot{y} + c\dot{y} + K_1 y + R(y) = A\cos(\Omega_1 t) + B\cos(\Omega_2 t), \tag{1}$$

where the restoring force $R(y)$ is piecewise linear, which is written as:

$$R(y)=\begin{cases}K_2(y-G) & , \quad y>G,\\ 0 & , \quad |y|\le G,\\ K_2(y+G) & , \quad y<-G,\end{cases} \tag{2}$$

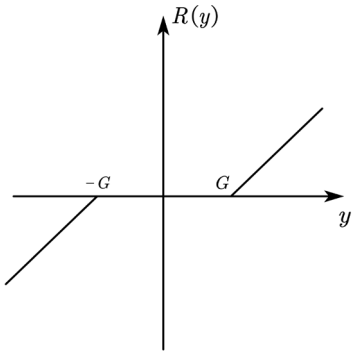

Fig. 2. Piecewise linear function $R(y)$.

and is shown in Fig. 2. The non-dimensional form of Eq. (1) is given as

$$\ddot{x}+2\xi\dot{x}+k_1x+F_r(x)=a\cos(\omega_1\tau)+b\cos(\omega_2\tau), \tag{3}$$

where $\tau=\Omega_n t$, $\Omega_n=\sqrt{K_1/m}$, $x=\frac{y}{y_0}$, $e=\frac{G}{y_0}$, $\xi=\frac{c}{2m\Omega_n}$, $a=\frac{A}{y_0mK_1}$, $b=\frac{B}{y_0mK_1}$ $k_1=\frac{K_1}{m}$, and $k_2=\frac{K_2}{m}$, and the ratio of ω_1 over ω_2 is an irrational number. $F_r(x)$ is the non-dimensional restoring force, which can be expressed as:

$$F_r(x)=\begin{cases}k_2(x-e) & , \quad x>e,\\ 0 & , \quad |x|\le e,\\ k_2(x+e) & , \quad x<-e.\end{cases} \tag{4}$$

As shown in Fig. 3, the double grazing bifurcation of quasiperiodic orbit means that the quasiperiodic torus have contacts with the two constraints *A* and *B* with zero velocity, which corresponds to the bottom and the top of the pothook contacts of the spring K_2 with zero velocity, respectively.

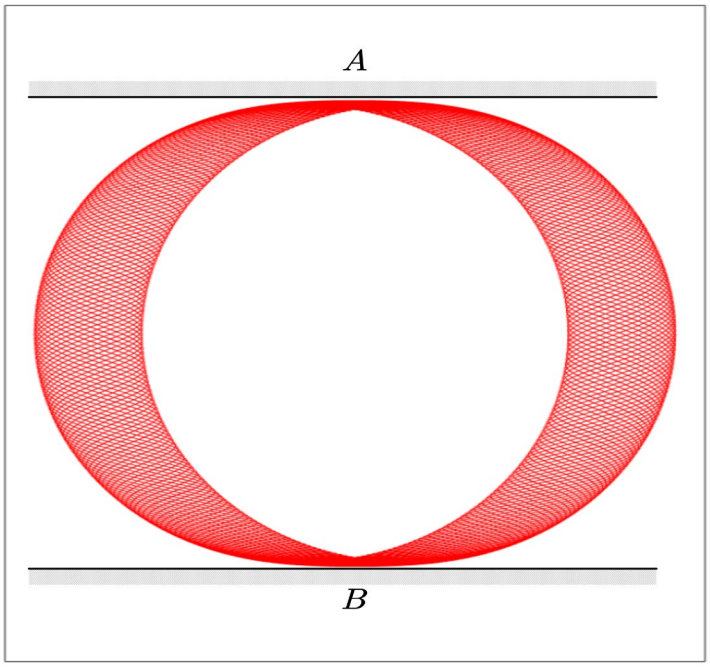

Fig. 3. Double grazing bifurcation of the quasiperiodic torus.

The quasiperiodic orbit can be determined analytically, and the maximum displacement for double grazing is obtained as

$$x_{\max} = \frac{a\sqrt{(S_1)^2 S_2} + b\sqrt{S_1 (S_2)^2}}{Z_1 Z_2 Z_3 Z_4}, \tag{5}$$

where $S_1 = 4\xi^2\omega_1^2 + k_1^2 - 2k_1\omega_1^2 + \omega_1^4$, $S_2 = 4\xi^2\omega_2^2 + k_1^2 - 2k_1\omega_2^2 + \omega_2^4$,

$Z_1 = 2\xi\sqrt{\xi^2 - k_1} - 2\xi^2 + k_1 - \omega_1^2$, $Z_2 = 2\xi\sqrt{\xi^2 - k_1} + 2\xi^2 - k_1 + \omega_1^2$, $Z_3 = 2\xi\sqrt{\xi^2 - k_1} - \xi^2 + k_1 - \omega_2^2$,

and $Z_4 = 2\xi\sqrt{\xi^2 - k_1} + 2\xi^2 - k_1 + \omega_2^2$.

Let $\theta = \omega_1 t$ and $\phi = \omega_2 t$, Eq. (3) can be transformed into the following state equations:

$$\begin{cases} \dot{x} = v, \\ \dot{v} = a\cos(\theta) + b\cos(\phi) - 2\xi v - k_1 x - F_r(x), \\ \dot{\theta} = \omega_1, \\ \dot{\phi} = \omega_2. \end{cases} \tag{6}$$

If ϕ is selected as the angle variable, we obtain the three-dimensional Poincaré map as follows:

$$\begin{aligned} &\Pi : \Sigma \to \Sigma : \\ &\Sigma \equiv \left\{ (x, v, \theta) \in R \times R \times S^1 \,|\, \phi \bmod 2\pi = 0 \right\}, \end{aligned} \tag{7}$$

which takes the form

$$\boldsymbol{f}:\boldsymbol{x}\to\boldsymbol{f}(\boldsymbol{x})=\begin{cases} x_{n+1}=\boldsymbol{f}_1\left(x_n,v_n,\phi_n\right), \\ v_{n+1}=\boldsymbol{f}_2\left(x_n,v_n,\phi_n\right), \\ \theta_{n+1}=\theta_n+2\pi\omega_1/\omega_2(\mathrm{mod}\,2\pi), \end{cases} \tag{8}$$

where x represents the displacement, and v denotes the velocity. In this paper, ω_2 takes the inverse of the golden mean value $(\sqrt{5}-1)/2$. Then the dynamics of the system is ergodic in the θ -axis. That is, the θ-axis is covered densely by the trajectory starting from any initial condition, which means that the Lyapunov exponent corresponding to the variable θ is always 0.

3. Characterization of SNAs

SNAs can be characterized by the Lyapunov exponents, phase sensitivity exponents, and power spectra [18,19].

Firstly, in order to describe the nonchaotic property of the SNAs, the Lyapunov exponents (i=1,2,3) is adopted as an effective method, which is given by

$$\lambda_i=\lim_{n\to\infty}\frac{1}{n}\sum_{k=0}^{n-1}\ln\left|\partial\boldsymbol{f}'(\boldsymbol{x})\right|. \tag{9}$$

For convenience, the maximum Lyapunov exponent is denoted by the symbol Λ in the following text. Then the attractor can be characterized as chaotic ($\Lambda>0$) or nonchaotic ($\Lambda\le 0$). If the value of Λ is non-positive, then the attractor is nonchaotic, which means that there is no sensitive dependence on initial conditions. It should be mentioned that the Lyapunov exponent corresponding to θ is always *0* due to the ergodicity in the θ -axis.

Secondly, the strange property of SNAs should be identified. Phase sensitivity is an effective tool to determine whether the attractor is strange or not, based on the sensitivity of the attractor to the phase of the external force [18,19]. There are some special tangent bifurcation points in SNAs, where the derivative of these bifurcation points with respect to the phase is infinite, indicating that the attractor is nonsmooth. The derivative of the attractor with respect to phase can be expressed as

$$S^N=\frac{\partial\boldsymbol{f}}{\partial\theta}, \tag{10}$$

where N is the number of iterations. If S^N tends to be infinite for $N\to+\infty$, the attractor is nonsmooth

and nondifferentiable, indicating that the attractor is strange [19] . For any small ε, we can select some n_0 to satisfy the phase difference condition $\varepsilon_0 = \left|\theta_{n_0} - \theta_0\right| < \varepsilon$, then the derivative of the attractor with respect to phase can be expressed approximately as

$$S^N = \frac{\partial \boldsymbol{f}}{\partial \theta} \approx \sum_{k=1}^{N-n_0} \left| \frac{\boldsymbol{f}\left(k+n_0\right) - \boldsymbol{f}(k)}{\theta\left(k+n_0\right) - \theta(k)} \right| = \sum_{k=1}^{N-n_0} \left| \frac{\boldsymbol{f}\left(k+n_0\right) - \boldsymbol{f}(k)}{\varepsilon_0} \right|, \tag{11}$$

where $k + n_0 \le N$, and $\boldsymbol{f}(k)$ denotes the kth iteration of $\boldsymbol{f}$. The maximum value of S^N after N iterations is the phase sensitivity function represented by

$$\tau^N = \max\left\{S^N\right\}, \tag{12}$$

which denotes the phase sensitivity index. If τ^N increases and tends to infinity with $N \to \infty$, the attractor has infinite derivative with respect to the external phase, demonstrating the strange property (i.e., non-smoothness). On the contrary, if τ^N increases but tends to a stable finite value with $N \to \infty$, then the attractor has no strange property due to the boundedness.

The strange property of the attractor can also be characterized by the power spectrum. When the orbit is periodic or quasiperiodic, the corresponding power spectrum is discrete, which is represented by δ-peaks at certain frequencies. The power spectrum is continuous if a system exhibits chaotic or random motions. However, for SNAs, a strange continuous spectrum appears between discrete and continuous spectrum [27]. The power spectrum given by iteration of the Poincaré map $\{x_n\}$ is defined by the discrete Fourier transform

$$X(\omega, N) = \sum_{n=1}^{N} x_n e^{i2\pi n\omega}. \tag{13}$$

Then, the power spectrum of the attractor is defined as [26]

$$P = \lim_{N\to\infty} \left| \frac{X(\omega, N)}{N} \right|^2 . \tag{14}$$

In addition, the power-law relation of $X(\omega, N)$ can be adopted to describe the strange property of SNAs. If the attractor is periodic or quasiperiodic, there is $|X(\omega, N)|^2 \sim N^2$. For chaotic attractor, the relation $|X(\omega, N)|^2 \sim N^1$ stands. If the attractor is an SNA, then the relation is described as [28]

$$|X(\omega, N)|^2 \sim N^{\beta}, \tag{15}$$

where $1 < \beta < 2$.

Moreover, the fractal structure of the attractor can be observed in the complex plane (*ReX, ImX*), indicating the strange property of SNAs [26, 29].

4. SNAs induced by double grazing of quasiperiodic orbits

In section 4 as to be discussed next, two cases of excitation are discussed. Firstly, in $b\cos(\omega_2\tau)$, the value of *b* is small (i.e., $b \ll a$). In these cases, $b\cos(\omega_2\tau)$ can be considered as a small perturbation. We show that in these cases SNAs may exist in a short parameter interval between 1T quasiperiodic orbit and 2T quasiperiodic orbit and between 1T quasiperiodic orbit and 4T quasiperiodic orbit, which are shown in section 4.1 and 4.2 respectively. However, if the value of *b* is zero, the SNAs cannot occurs.

Secondly, for larger *b* (i.e., general quasiperiodic excitation), SNAs induced by the double grazing may exist in a large parameter interval, between quasiperiodic orbit and chaotic motion, which are shown in section 4.3 and 4.4 respectively.

4.1 SNAs between 1T torus and 2T torus after double grazing bifurcation

The system parameter combination (1): $a = 0.3$, $b = 1\times10^{-6}$, ξ=0.5, ω_1=5, $k_1 = 1$, $k_2 = 200$ is selected, and clearance e is chosen as the control parameter. The maximum displacement for double grazing bifurcation of quasiperiodic orbit is computed as $e^* \approx 1.2238\times10^{-2}$ according to Eq. (5). As shown in Fig. 4, the bifurcation diagram and the maximum Lyapunov exponent can be obtained numerically (the zero Lyapunov exponent in the θ -direction is removed). The maximal Lyapunov exponent is negative in the whole parameter interval, which denotes that no chaos is present in the interval. As the parameter value is $e \geq e^*$, the system exhibits quasiperiodic 1T orbit, corresponding to the blue area in Figs. 4 (a) and (b). If e is smaller than the critical value e^* (i.e., $e^1 < e < e^*$), the torus become nonsmooth due to the double grazing bifurcation, corresponding to the red area in Figs. 4 (a) and (b). As the parameter e decreases further (i.e., $e^2 < e < e^1$), the SNAs appear, in correspondence with the gray area in Figs. 4 (a) and (b). However, as the value of the parameter e decreases further (i.e., $e^3 < e < e^2$), SNAs evolve into nonsmooth 2T quasiperiodic torus, which is in correspondence with the red area of Figs.

4 (a) and (b). Finally, when the parameter is decrease to e^3, the system exhibits smooth 2T quasiperiodic torus, corresponding to the green area in Figs. 4 (a) and (b). In summary, in this case, double grazing-induced SNAs exist in a short parameter interval between 1T quasiperiodic orbit and 2T quasiperiodic orbit.

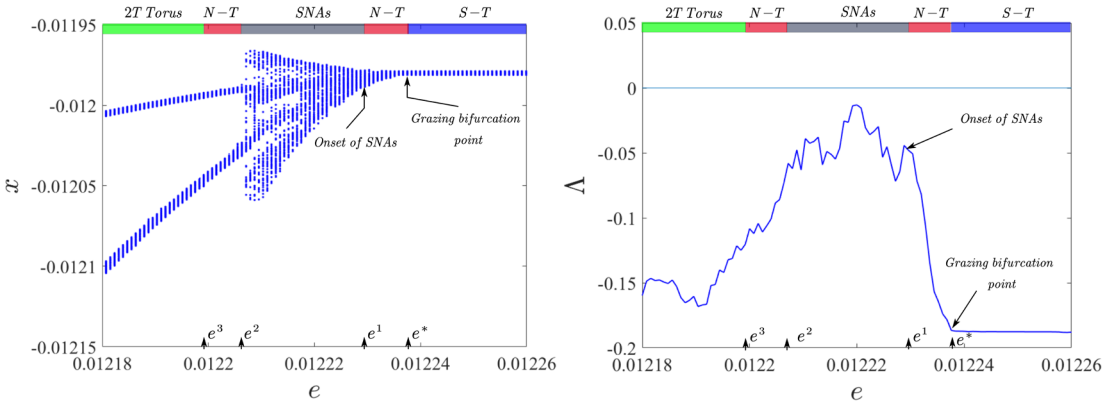

(a) (b)

Fig. 4. SNAs between 1T torus and 2T torus after double grazing. (a) Bifurcation diagram. (b) The maximal Lyapunov exponent diagram with the variation of e. The labels *S-T* and *N-T* denote a smooth torus and a nonsmooth torus, respectively.

The phase diagrams are shown in Fig. 5, indicating the transition from quasiperiodic attractors to SNAs through the double grazing bifurcation route. As $e=1.224\times10^{-2}$, the system exhibits a smooth quasiperiodic smooth 1T torus in the coordinate plane (x_n, v_n) of the Poincaré section, as shown in Fig. 5 (a). When e decreases to $e^* \approx 1.2238\times10^{-2}$, the double grazing bifurcation occurs on the torus. Subsequently, the smooth 1T torus becomes wrinkled and "non-differentiable", whose onset is shown in Fig. 5 (b). As the value of the parameter e decreases to $e=1.222\times10^{-2}$, the 1T torus exhibits the loss of smoothness even further as an SNA, as shown in Fig. 5 (c). Finally, when the parameter decreases to $e=1.219\times10^{-2}$, SNAs settle into the 2T quasiperiodic torus, as shown in Fig. 5 (d).

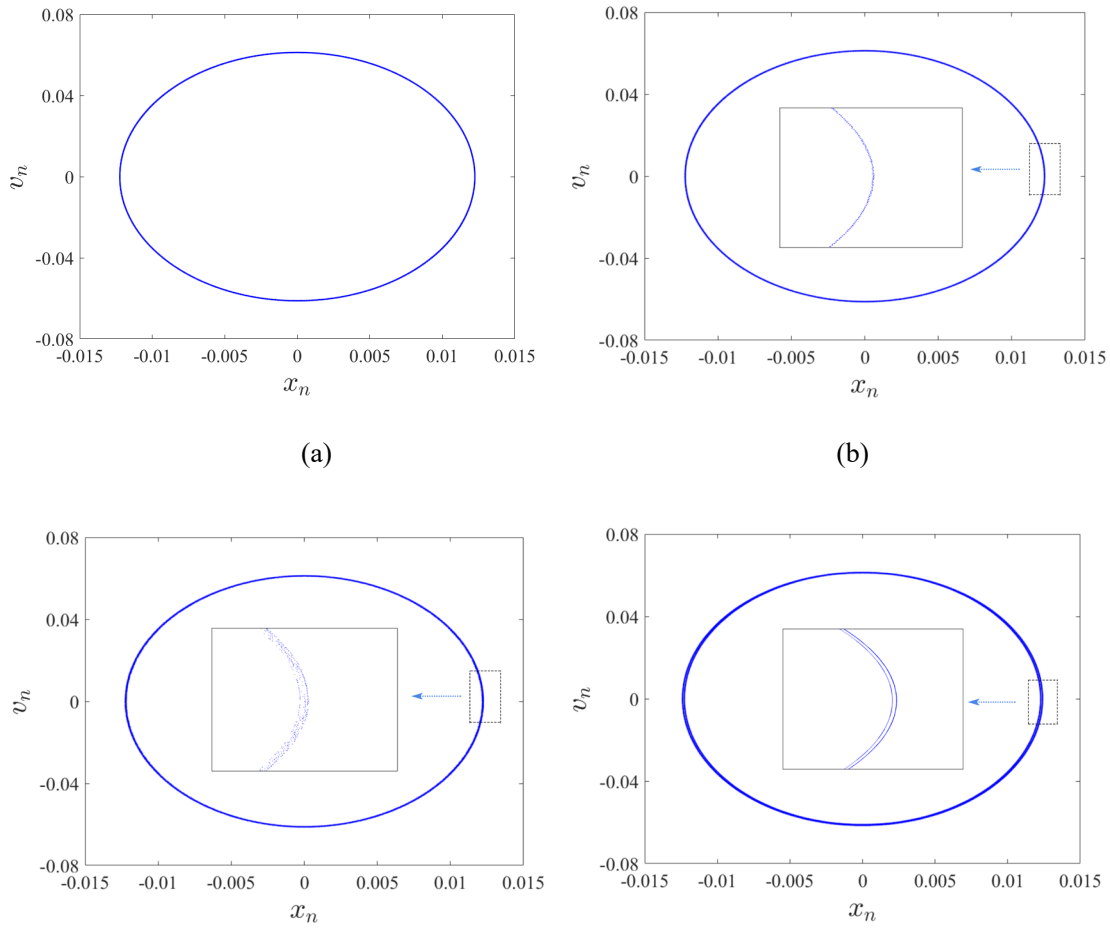

Fig. 5. Phase diagrams of the Poincaré section for parameter combination (1).

(a) $e=1.224\times10^{-2}$: smooth 1T torus; (b) $e=1.2235\times10^{-2}$: nonsmooth 1T torus;

(c) $e=1.222\times10^{-2}$: SNA; (d) $e=1.219\times10^{-2}$: 2T torus.

4.2 SNAs between 1T torus and 4T torus after double grazing bifurcation

As a second system parameter combination (2): $a=0.3$, $b=2\times10^{-6}$, ξ=0.525, ω_1=7.25, $k_1=1$, $k_2=200$ is selected, and clearance e is chosen as the control parameter. The maximum displacement for double grazing bifurcation of the quasiperiodic orbit is computed as $e^*\approx5.758\times10^{-3}$. The bifurcation diagram and the maximum Lyapunov exponent are shown in Fig. 6. Chaos does not appear in the whole parameter interval as the maximal Lyapunov exponent converges to negative values. When the parameter value is $e\geq e^*$, the system exhibits the quasiperiodic 1T torus, corresponding to the blue area in Figs. 6 (a) and (b). However, if e is

smaller than the critical value e^* (i.e., $e^1 < e < e^*$), the torus begins to wrinkle and to lose its smoothness due to double grazing bifurcation , corresponding to the red area in Figs. 6 (a) and (b). As the parameter e decreases further (i.e., $e^2 < e < e^1$), the torus loses its smoothness completely and evolves into SNAs, which is in correspondence with the gray area in Figs. 6 (a) and (b). However, as the value of the parameter e decreases further (i.e., $e^3 < e < e^2$), SNAs evolve into the nonsmooth 4T torus, which is in correspondence with the red area of Figs. 6 (a) and (b). Finally, when the parameter is decrease to e^3, the system settles into 4T torus corresponding to the green area in Figs. 6 (a) and (b). In this case, double grazing-induced SNAs exist in a short parameter interval between 1T quasiperiodic torus and 4T quasiperiodic torus.

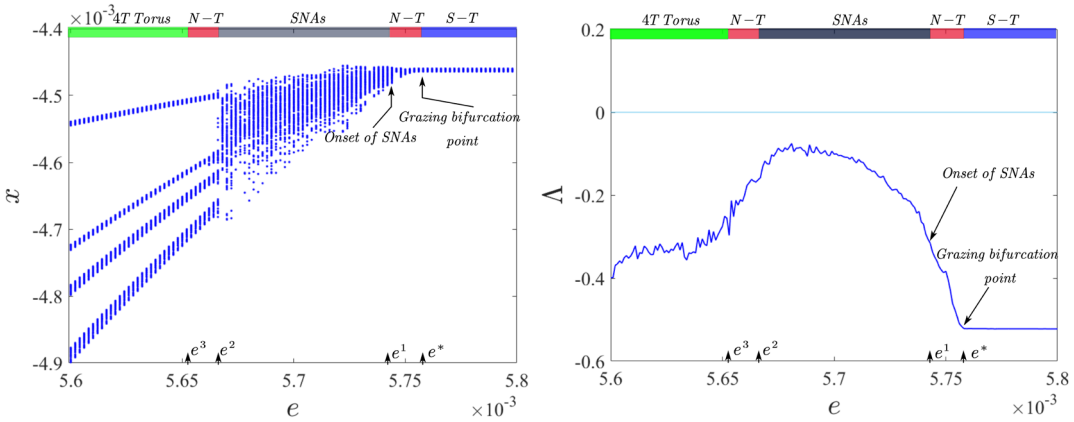

(a) (b)

Fig. 6. SNAs between 1T torus and 4T torus. (a) Bifurcation diagram. (b) The maximal Lyapunov exponent diagram with the variation of e.

The phase diagrams changing with the values of e are shown in Fig. 7. Fig. 7 (a) shows the smooth 1T torus as $e = 5.76 \times 10^{-3}$. As the parameter e reaches the critical value $e^* \approx 5.758 \times 10^{-3}$, the smooth 1T torus begins to fold and becomes nonsmooth because of the double grazing bifurcation. As the parameter e decreases to $e = 5.75 \times 10^{-3}$, the smooth 1T torus becomes a non-smooth 1T torus, as shown as Fig. 7 (b). As the parameter e decreases to $e = 5.7 \times 10^{-3}$, the SNA is generated and is shown as Fig. 7 (c). Finally, when the parameter decreases to $e = 5.63 \times 10^{-3}$, the system settles into the 4T quasiperiodic torus, as shown in Fig. 7 (d).

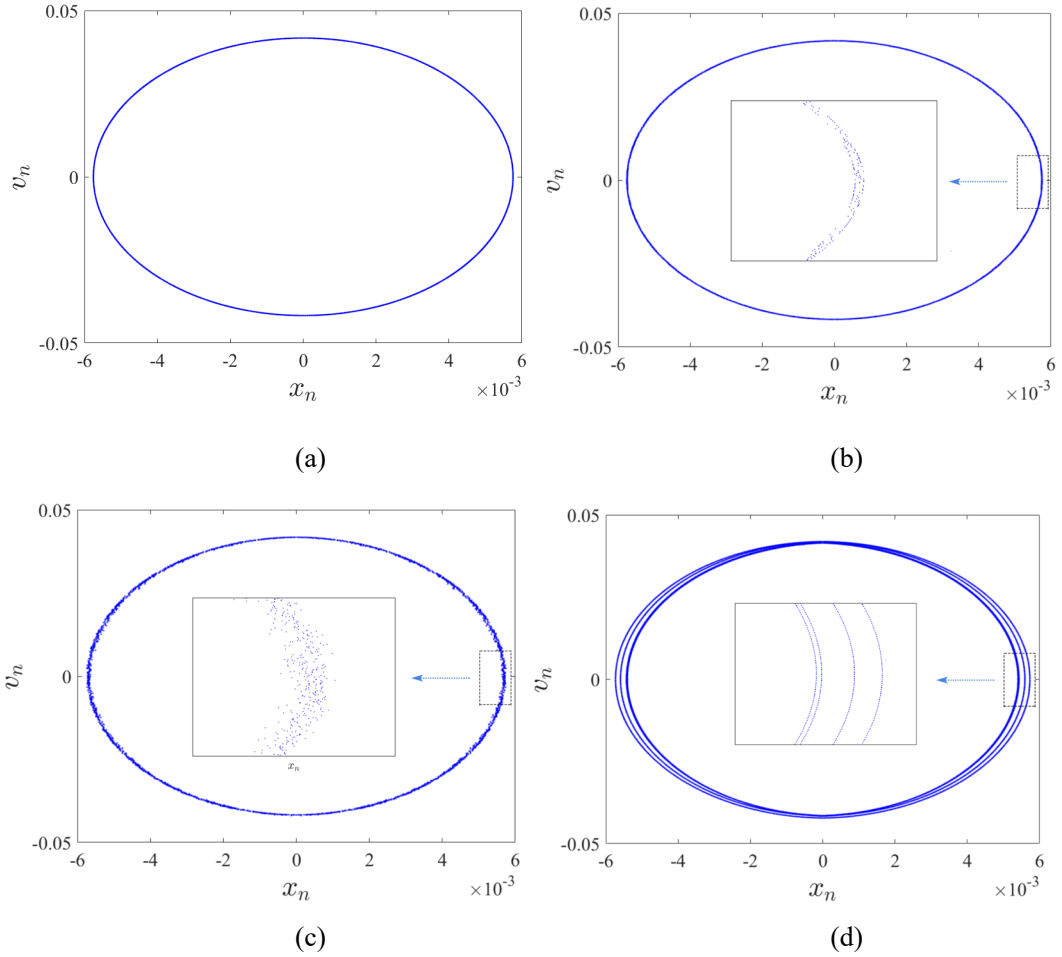

Fig. 7. Phase diagrams of the Poincaré section for parameter combination (2). (a) $e = 5.76 \times 10^{-3}$: smooth 1T torus; (b) $e = 5.75 \times 10^{-3}$: nonsmooth 1T torus; (c) $e = 5.7 \times 10^{-3}$: SNA; (d) $e = 5.63 \times 10^{-3}$: 4T torus.

4.3 SNAs between 1T torus and chaos after double grazing bifurcation

The third system parameter combination (3): $a = b = 5$, ξ=0.01, ω_1=1, $k_1 = 0.3$, $k_2 = 100$ is selected, and the clearance e is again chosen as the control parameter. The maximum displacement for the double grazing bifurcation of the quasiperiodic orbit is obtained as $e^* \approx 67.4588$. The bifurcation diagram and the maximal Lyapunov exponent Λ varying with the parameter e are shown in Figs. 8 (a) and (b) respectively. When the parameter $e \geq e^*$, the system exhibits quasiperiodic 1T torus, which corresponds to the blue area of Figs. 8 (a) and (b). As shown in Fig. 8 (b), the maximal Lyapunov exponent Λ converges to a negative value. However, after the

double grazing bifurcation ($e^1 < e < e^*$), the 1T torus begins to wrinkle, losing its smoothness gradually. As the value of the parameter e decreases further (i.e., $e^2 < e < e^1$), the torus loses its smoothness completely and becomes an SNA, the maximal Lyapunov exponent is still negative which is in correspondence with the gray area of Figs. 8 (a) and (b). Finally, when the parameter is decreased to e^2 , the system exhibits chaotic motion, and the maximal Lyapunov exponent is positive, as shown in the black area of Figs. 8 (a) and (b), respectively. In summary, in this case, double grazing-induced SNAs exist in a short parameter interval between the quasiperiodic 1T torus and chaotic attractor. For the SNAs, the nonchaotic property is determined by means of the maximal Lyapunov exponent in Fig.8 (b), and the strange property will be verified in the next section.

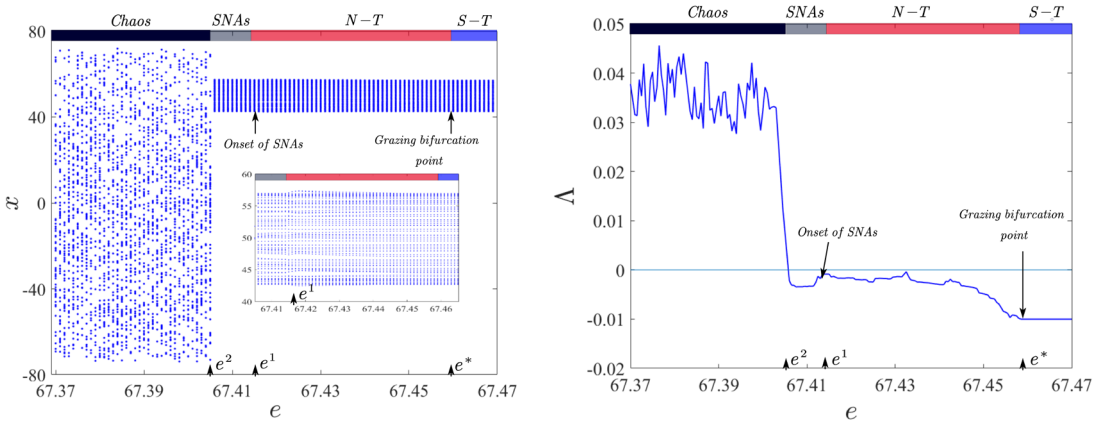

(a) (b)

Fig. 8. SNAs between 1T torus and chaos. (a) Bifurcation diagram. (b) The maximal Lyapunov exponent diagram with the variation of e .

The phase diagrams in the Poincaré section are shown in Fig. 9. As $e = 67.46$, the system exhibits a smooth torus in the Poincaré section, as shown in Fig. 9 (a). When e decreases to $e^* \approx 67.4588$, the double grazing bifurcation occurs on the torus. Subsequently, the smooth 1T torus becomes wrinkled and nonsmooth, as shown in Fig. 9 (b). As the value of the parameter e decreases further, more and more nonsmooth points appear, as shown in Fig. 9 (c). Finally, when e decreases to $e = 67.407$, the 1T torus becomes extremely wrinkled and loses the smoothness completely, evolving into SNAs, as shown in Fig. 9 (d).

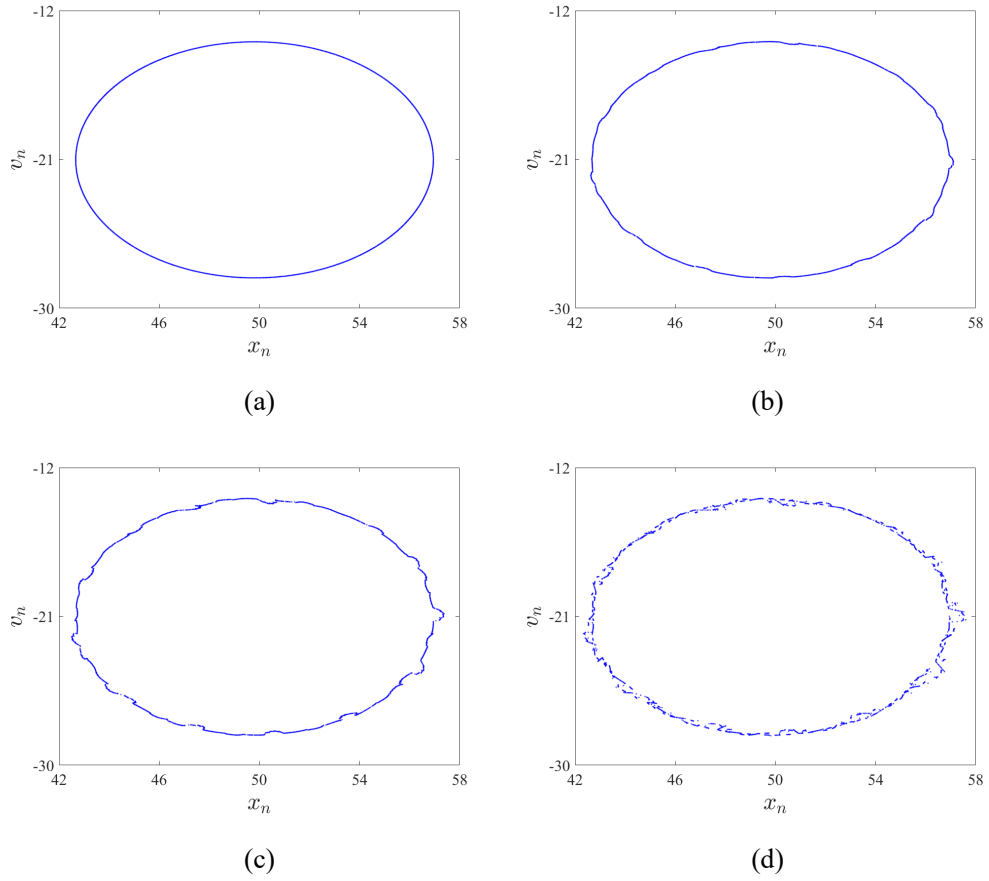

Fig. 9. Phase diagrams of the Poincaré section for parameter combination (3).

(a) $e = 67.46$: smooth 1T torus; (b) $e = 67.44$: nonsmooth 1T torus;

(c) $e = 67.42$: nonsmooth 1T torus; (d) $e = 67.407$: SNA.

4.4 SNAs in a long parameter interval after double grazing bifurcation

As the fourth system parameter combination (4): a=b=4 , ξ=0.02 , ω_1=1, $k_1 = 0.4$, $k_2 = 32$ is selected, and e is chosen as the control parameter. The maximum displacement of quasiperiodic orbit is obtained as $e^* \approx 137.37$, indicating the critical value of the double grazing bifurcation. As shown in Fig. 10, the bifurcation diagram and the maximum Lyapunov exponent can be obtained numerically. When the parameter value is $e \geq e^*$, the system exhibits quasiperiodic 1T torus, corresponding to the blue area in Figs. 10 (a) and (b). If e is smaller than the critical value $e^* \approx 137.37$ (i.e., $e^1 < e < e^*$), the 1T torus becomes nonsmooth due to the double grazing bifurcation, corresponding to the red area in Figs. 10 (a) and (b). As the parameter e decreases further (i.e., $e < e^1$), the SNAs are generated, in correspondence with the gray area in Figs. 10 (a)

and (b). Here the process from a quasiperiodic attractor to an SNA is similar to the third parameter combination, however, the difference is that the SNA does not lead to chaos as parameter is changed. Consequently, the maximal Lyapunov exponent converges to a negative value in the whole parameter interval, as shown in Fig. 10 (b). In the interval $e < e^1$, the strange property will be verified in the next section.

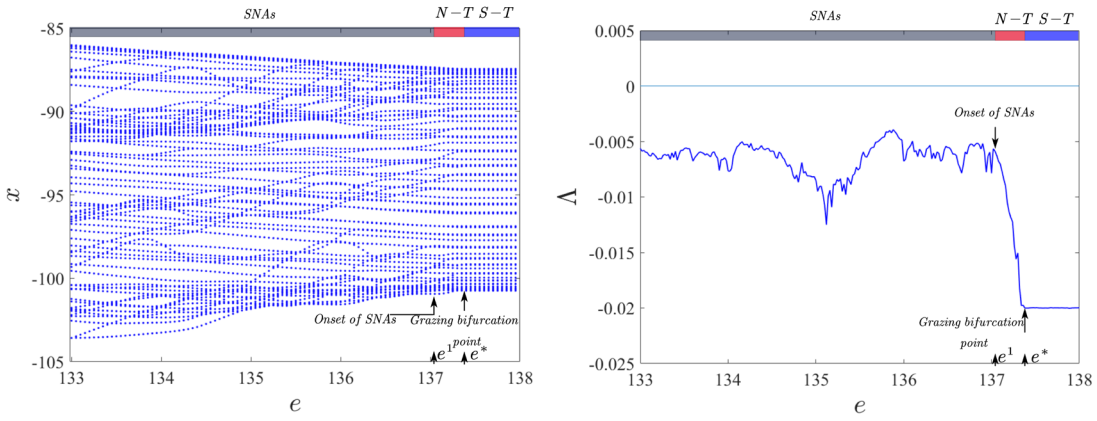

（a） （b）

Fig. 10. SNAs induced by double grazing bifurcation. (a) Bifurcation diagram. (b) The maximal Lyapunov exponent diagram with the variation of e.

In the case of parameter combination (4), the phase diagrams of the Poincaré section are shown in Fig. 11. Figure 11 (a) shows the quasiperiodic attractor for $e = 137.4$. As the parameter e goes slightly across the critical value $e^* \approx 137.37$, the smooth torus begins to fold and becomes nonsmooth after double grazing bifurcation, as shown in Fig. 11 (b). As the parameter e decreases to $e = 136.9$, a SNA is generated as shown in Fig. 11 (c). When the bifurcation parameter is far from the grazing bifurcation point e^*, the attractor is still strange and has nonchaotic properties, as shown in Fig. 11 (d). Here, SNAs induced by double grazing bifurcation exist in a large parameter range after grazing.

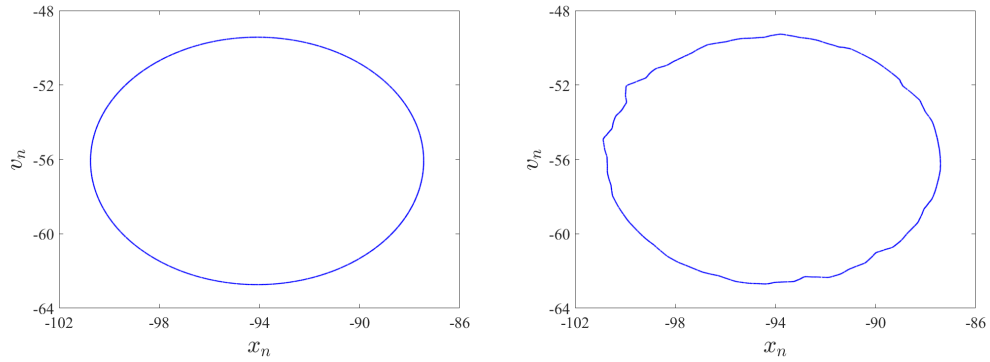

(a) (b)

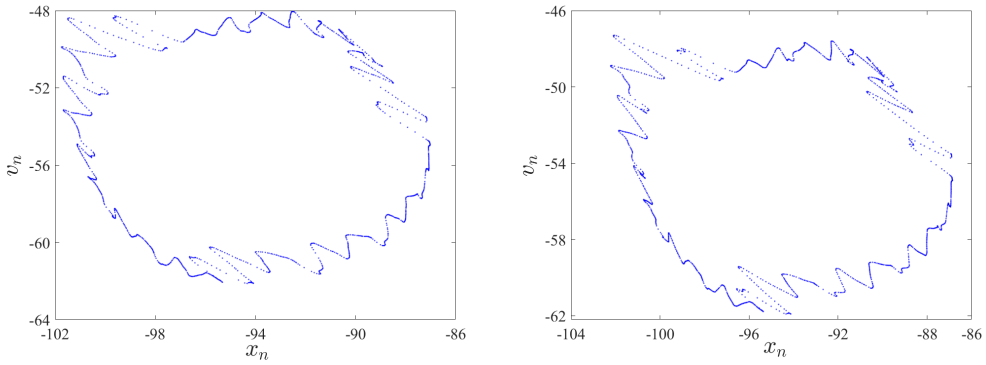

(c) (d)

Fig. 11. Phase diagrams of the Poincaré section for parameter combination (4).

(a) $e = 137.4$: smooth 1T torus; (b) $e = 137.2$: nonsmooth 1T torus; (c) $e = 136.9$: SNA; (d) $e = 135.5$: SNA.

5. Characterizing the Strange Property of SNAs

The strange property can be effectively characterized by the phase sensitivity [18,19]. For SNAs, the derivate of the dynamics on the attractor with respect to phase tends to infinite, indicating the nondifferentiability of the attractor. Further, the attractor is not strange. In the case of parameter combination (3), Fig. 12(a) presents the diagram of phase sensitivity functions for both SNA and torus. For the SNA shown in Fig. 9 (d), as the number of iterations increases, the value of τ^N tends to infinity, which corresponds to the red curve in Fig. 12 (a). For the quasiperiodic torus shown in Fig. 9 (a), as the number of iterations increases, the value of τ^N tends to a bounded value, corresponding to the blue curve in Fig. 12 (a). For the parameter combination (4), Fig. 12 (b) presents the phase sensitivity functions for both SNA and torus. For the SNA shown in Fig. 11 (c), with increasing the iteration number, the value of τ^N tends to infinity, corresponding to the red curve in Fig. 12 (b), indicating the strange property of the attractor. However, the value of τ^N is bounded for the torus shown in Fig. 11 (a), as exhibited by the blue curve in Fig. 12 (b).

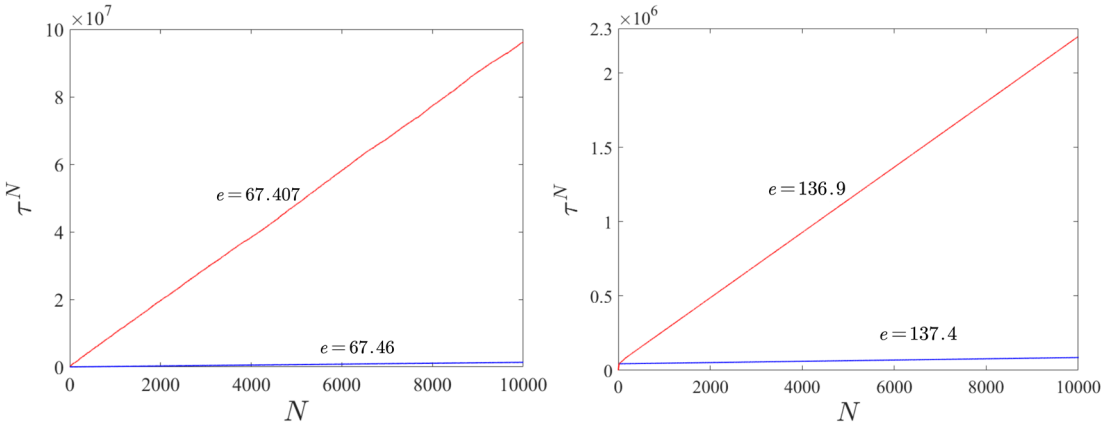

(a) (b)

Fig. 12. Phase sensitivity functions of the torus and the SNA; (a) corresponding to Fig. 9 (a) and Fig. 9 (d); (b) corresponding to Fig. 11 (a) and Fig. 11 (c).

The power spectrum plays an important role in characterizing SNAs. Because SNAs exhibit a dynamical property between regular and irregular, the power spectrum of the SNA is a mixture of both discrete and continuous spectra. Taking the SNA in Fig. 9 (d) as an example, Fig. 13 (a). shown that the power spectrum is continuous, and that it has δ peaks at some frequencies, indicating that the attractor has both strange and nonchaotic characteristics. The scaling exponent $\beta \approx 1.77$ can be obtained by calculating the power-law relation according to Eq. (14). The exponent β satisfies the power-law relation ($1 < \beta < 2$) for large N, as shown in Fig. 13 (b). Additionally, the spectral trajectory in the complex plane of (*ReX, ImX*) exhibits the fractal structure as in Fig. 13 (c), which also characterizes the strange property of SNA.

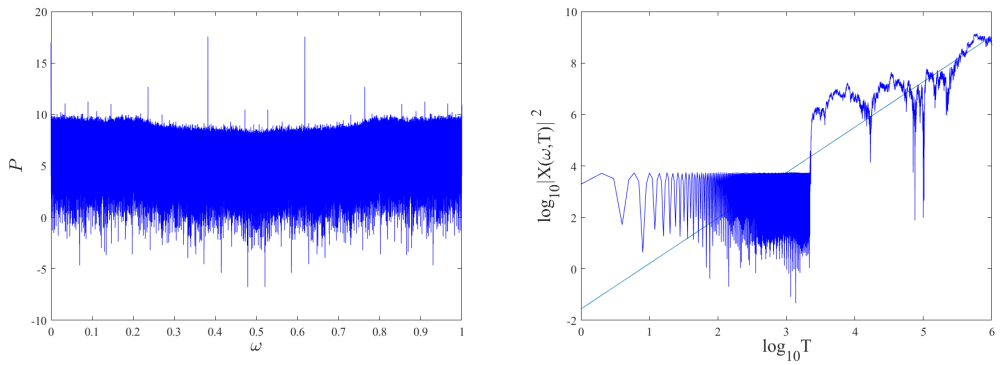

(a) (b)

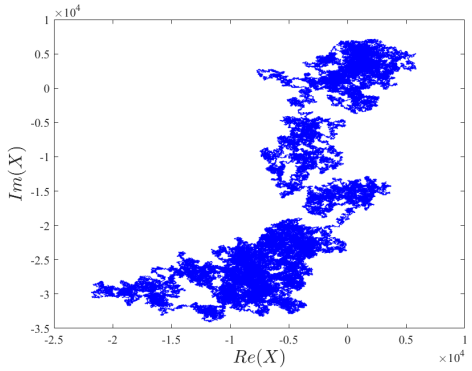

(d)

Fig. 13. Characterizing the strangeness of the SNA in Fig. 9 (d). (a) The power spectrum. (b) Singular continuous spectrum. (c) The fractal structure of trajectories in the complex plane (*ReX, ImX*).

Now the strange property of the SNA in Fig. 11(c) is verified by the power spectrum, singular continuous spectrum, and fractal graph, as shown in Fig. 14. Numerous δ peaks can be seen in the power spectrum diagram in Fig. 14 (a), exhibiting an appearance which is both discrete and continuous semblance. On the other hand, the power-law relation in Fig. 14 (b) is $|X(\omega,N)|^2 \sim N^{1.56}$, which means that the attractor is strange. Furthermore, the fractal structure of the trajectories in complex plane (*ReX, ImX*) is exhibited in Fig. 14 (c), indicating the strange property of the attractor.

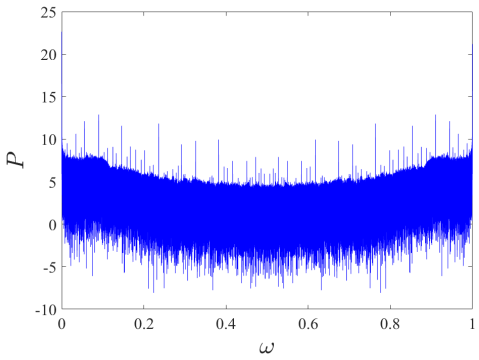

(a)

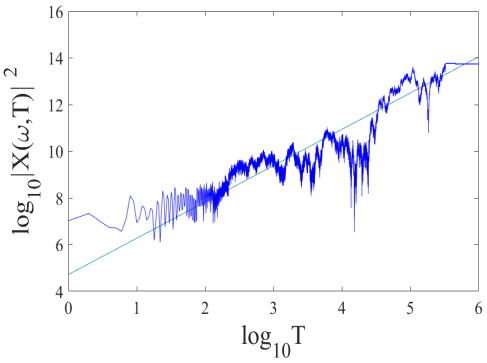

(b)

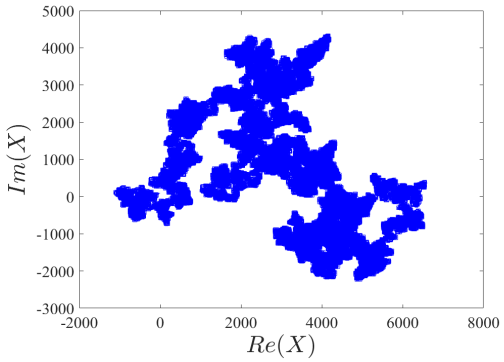

(c)

Fig. 14. Characterizing the strange of the SNA in Fig. 11 (c). (a) The power spectrum. (b) Singular continuous spectrum. (c) The fractal structure of trajectories in the complex plane (*ReX, ImX*).

6. Conclusions

A piecewise linear oscillator with quasiperiodic excitation is considered in this work. It led to a new bifurcation, the creation of SNAs through the double grazing bifurcation route of quasiperiodic torus. Firstly, the expression of the maximum displacement of the quasiperiodic torus is given to determine the double grazing bifurcation point. Subsequently, we obtain the bifurcation diagram, maximal Lyapunov exponents diagram, and the phase diagram of Poincaré section. The nonchaotic property of SNAs is characterized by the maximal Lyapunov exponent, and the strange property is verified by phase sensitive function, power spectrum, singular continuous spectrum, and fractal graph. The results show that the SNAs induced by double grazing may exist in a short parameter interval between 1T quasiperiodic orbit and 2T quasiperiodic orbit, or between 1T quasiperiodic orbit and 4T quasiperiodic orbit, or between 1T quasiperiodic orbit and chaotic motion. In addition, SNAs may also exist in a large parameter interval after double grazing without leading to any quasiperiodic motion or chaos.

Acknowledgments

This work is supported by the National Natural Science Foundation of China (NNSFC) (Nos. 12072291, 11732014, and 12172306).

References

[1] Whiston G S. Global dynamics of a vibro-impacting linear oscillator. Journal of Sound and Vibration, 1987, 118(3): 395-424.

[2] Whiston G S. Singularities in vibro-impact dynamics. Journal of Sound and Vibration, 1992, 152(3): 427-460.

[3] Shaw S W, Holmes P J. A periodically forced piecewise linear oscillator. Journal of Sound and Vibration, 1983, 90(1): 129-155.

[4] Chillingworth D R J. Discontinuity geometry for an impact oscillator. Dynamical Systems, 2002, 17(4): 389-420.

[5] Chillingworth D R J. Dynamics of an impact oscillator near a degenerate graze. Nonlinearity, 2010, 23(11): 2723.

[6] Jiang H B, Wiercigroch M. Geometrical insight into non-smooth bifurcations of a soft impact oscillator. IMA Journal of Applied Mathematics, 2016, 81(4): 662- 678.

[7] Kryzhevich S G. Grazing bifurcation and chaotic oscillations of vibro-impact systems with one degree of freedom. Journal of Applied Mathematics and Mechanics, 2008, 72: 383-390.

[8] Banerjee S, Ing J, Pavlovskaia E, et al. Invisible grazings and dangerous bifurcations in impacting systems: the problem of narrow-band chaos. Physical Review E, 2009, 79(3): 037201.

[9] Yin S, Wen G L , Ji J C, Xu H D. Novel two-parameter dynamics of impact oscillators near degenerate grazing points. International Journal of Non-Linear Mechanics, 2020, 120: 103403.

[10] Nordmark A B. Non-periodic motion caused by grazing incidence in an impact oscillator. Journal of Sound and Vibration, 1991, 145(2): 279-297.

[11] Nordmark A B. Universal limit mapping in grazing bifurcations. Physical Review E, 1997, 55(1): 266–270.

[12] Chin W, Ott E, Nusse H E, et al. Grazing bifurcations in impact oscillators. Physical Review E, 1994, 50(6): 4427.

[13] Dankowicz H, Zhao X P. Local analysis of co-dimension-one and co-dimension-two grazing bifurcations in impact microactuators. Physica D, 2005, 202(3-4): 238-257.

[14] Zhang S J, Lu Q S. A non-smooth analysis to the rub-impacting rotor system. Acta

mechanica sinica, 2000, 32(1): 59-69.

[15] Feng J Q, Xu W. Grazing-induced chaotic crisis for periodic orbits in vibro-impact systems. Acta mechanica sinica, 2013, 45(1): 30-36.

[16] Brzeski P, Chong A S E, Wiercigroch M, et al. Impact adding bifurcation in an autonomous hybrid dynamical model of church bell. Mechanical Systems and Signal Processing, 2018, 104: 716-724.

[17] Grebogi C, Ott E, Pelikan S, Yorke J. Strange attractors that are not chaotic. Physica D, 1984, 13(1): 261-268.

[18] Feudel U, Kuznetsov S, Pikovsky A. Strange nonchaotic attractors: dynamics between order and chaos in quasiperiodically forced systems. Singapore: World Scientific , 2006.

[19] Pikovsky A, Feudel U. Characterizing strange nonchaotic attractors. Chaos, 1995, 5(1): 253-260.

[20] Glendinning P, Jäger T, Keller G. How chaotic are strange nonchaotic attractors. Nonlinearity, 2006, 19(9): 2005-2022.

[21] Mitsui T, Aizawa Y. Intermittency route to strange nonchaotic attractors in a non-skew-product map. Physical Review E, 2010, 81(4): 046210.

[22] Zhang G J, Wang J, Xu J X, et al. Strange non-chaotic attractors in noisy FitzHugh-Nagumo neuron model. Springer Netherlands, 2011.

[23] Li G L, Yue Y, Grebogi C, et al. Strange nonchaotic attractors in a periodically forced piecewise linear system with noise. Fractals, 2021, 30(1): 2250003.

[24] Shen Y, Zhang Y. Mechanisms of strange nonchaotic attractors in a nonsmooth system with border-collision bifurcations. Nonlinear Dynamics, 2019, 96(2): 1405-1428.

[25] Zhang Y, Shen Y. A new route to strange nonchaotic attractors in an interval map. International Journal of Bifurcation and Chaos, 2020, 30(4): 2020063.

[26] Yalçinkaya T, Lai Y C. Blowout bifurcation route to strange nonchaotic attractors. Physical Review Letters, 1996, 77(25): 5039-5042.

[27] Pikovsky A, Zaks M, Feudel U, Kurths J. Singular continuous spectra in dissipative dynamics. Physical Review E, 1995, 52(1): 285–96.

[28] Jalnine A Y, Kuznetsov S P. Autonomous strange non-chaotic oscillations in a system of mechanical rotators. Regular Chaotic Dynamics, 2017, 22(3): 210–225.

[29] Yalçinkaya T, Lai Y C. Bifurcation to strange nonchaotic attractors. Physical Review E, 1997, 56(2):1623-1630.